Guided-mode resonance photonic crystal slab sensors based on bead monolayer geometry

Lina Shi, Pierre Pottier, Yves-Alain Peter and Maksim Skorobogatiy

Engineering Physics Department, Ecole Polytechnique de Montréal, Montréal (QC) H3C 3A7, Canada

lina.shi@polymtl.ca

Abstract: Using finite-difference time-domain method, we investigate photonic crystal slabs consisting of spherical voids or silica beads embedded into a dielectric slab as bio-chemical sensors. We study the dependence of the spectral position of guided-mode resonances on the refractive index of a slab material. The most sensitive design is based on voids filled with analyte. We also study the effects of the slab and analyte thicknesses on guided-mode resonance properties. We eventually demonstrate an aqueous analyte sensor with high sensitivity at visible wavelength as electro-magnetic energy distribution in some guided-mode resonances can be strongly localized in the analyte region.

OCIS codes: (130.6010) Sensors; (050.5298) Photonic crystals; (260.5740) Resonance; (230.3990) Micro-optical devices.

References and links

1. W. Lukosz, "Principle and sensitivities of integrated optical and surface plasmon sensors for direct affinity sensing and immunosensing," Biosens. Bioelectron. **6**, 215-225 (1991).
2. J. Homola, *Surface Plasmon Resonance Based Sensors* (Springer, 2006).
3. B. Gauvreau, A. Hassani, M. F. Fehri, A. Kabashin, and M. A. Skorobogatiy, "Photonic bandgap fiber-based Surface Plasmon Resonance sensors," Opt. Express **15**, 11413-11426 (2007).
4. R. Magnusson, and S. S. Wang, "New principle for optical filters," Appl. Phys. Lett. **61**, 1022-1024 (1992).
5. S. Peng and G. M. Morris, "Resonant scattering from two-dimensional gratings," J. Opt. Soc. Am. A **13**, 993-1005 (1996).
6. M. Kanskar, P. Paddon, V. Pacradouni, R. Morin, A. Busch, J. F. Young, S. R. Johnson, J. MacKenzie, and T. Tiedje, "Observation of leaky slab modes in an air-bridged semiconductor waveguide with a two-dimensional photonic lattice," Appl. Phys. Lett. **70**, 1438-1440 (1997).
7. M. Boroditsky, R. Vrijen, T. F. Krauss, R. Coccioli, R. Bhat, and E. Yablonovitch, "Spontaneous emission extraction and Purcell enhancement from thin-film 2-D photonic crystals," J. Lightwave Technol. **17**, 2096-2112 (1999).
8. V. N. Astratov, I. S. Culshaw, R. M. Stevenson, D. M. Whittaker, M. S. Skolnick, T. F. Krauss, and R. M. De la Rue, "Resonant coupling of near-infrared radiation to photonic band structure waveguides," J. Lightwave Technol. **17**, 2050-2057 (1999).
9. V. Pacradouni, W. J. Mandeville, A. R. Cowan, P. Paddon, and J. F. Young, "Photonic band structure of dielectric membranes periodically textured in two dimensions," Phys. Rev. B, **62**, 4204-4206 (2000).
10. A. R. Cowan, P. Paddon, V. Pacradouni, and J. F. Young, "Resonant scattering and mode coupling in two dimensional textured planar waveguides," J. Opt. Soc. Am. A **18**, 1160-1170 (2001).
11. S. Fan and J. D. Joannopoulos, "Analysis of guided resonances in photonic crystal slabs," Phys. Rev. B **65**, 235112 (2002).
12. M. Szekeres, O. Kamalin, R. A. Schoonheydt, K Wostyn, K. Clays, A. Persoonsc, and I. Dékány, "Ordering and optical properties of monolayers and multilayers of silica spheres deposited by the Langmuir Blodgett method," J. Mater. Chem. **12**, 3268-3274 (2002).

#101181 - $15.00 USD Received 5 Sep 2008; revised 17 Oct 2008; accepted 17 Oct 2008; published 21 Oct 2008

13. W. Suh, M. F. Yanik, O. Solgaard, and S. Fan, "Displacement-sensitive photonic crystal structures based on guided resonance in photonic crystal slabs," Appl.Phys.Lett. **82**, 1999-2001 (2003).
14. O. Kilic, S. Kim, W. Suh, Y. Peter, A. S. Sudb03, M. F. Yanik, S. Fan, and O. Solgaard, "Photonic crystal slabs demonstrating strong broadband suppression of transmission in the presence of disorders," Opt. Lett. **29**, 2782-2784 (2004).
15. V. Lousse, W. Suh, O. Kilic, S. Kim, O. Solgaard, and S. Fan, "Angular and polarization properties of a photonic crystal slab mirror," Opt. Express **12**, 1575-1582 (2004).
16. L. Landström, D. Brodoceanu, N. Arnold, K. Piglmayer, and D. Bäuerle, "Photonic properties of silicon-coated colloidal monolayers," Appl. Phys. A **81**, 911-913 (2005).
17. A. Rosenberg, M. W. Carter, J. A. Casey, M. Kim, R. T. Holm, R. L. Henry, C. R. Eddy, V. A. Shamamian, and K. Bussmann, "Guided resonances in asymmetrical GaN photonic crystal slabs observed in the visible spectrum," Opt. Express **13**, 6564-6571 (2005).
18. K. B. Crozier, V. Lousse, O. Kilic, S. Fan, and O. Solgaard, "Air-bridged photonic crystal slabs at visible and near-infrared wavelengths," Phys. Rev. B **73**, 115126 (2006).
19. Z. Jian and D. M. Mittlemana, "Characterization of guided resonances in photonic crystal slabs using terahertz time-domain spectroscopy," J. Appl. Phys. **100**, 123113-123118 (2006).
20. T. Prasad, V. L. Colvin, and D. M. Mittleman, "The effect of structural disorder on guided resonances in photonic crystal slabs studied with terahertz time-domain spectroscopy," Opt. Express **15**, 16954-16965 (2007).
21. J. L. Skinner, A. A. Talin, and D. A. Horsley, "A MEMS light modulator based on diffractive nanohole gratings," Opt. Express **16**, 3701-3711 (2008).
22. L. Prodan, R. Hagen, P. Gross, R. Arts, R. Beigang, C. Fallnich, A. Schirmacher, L. Kuipers, and K-J Boller,"Mid-IR transmission of a large-area 2D silicon photonic crystal slab," J. Phys. D: Appl. Phys. **41**, 135105-135111 (2008).
23. Y. Nazirizadeh, J. G. Mller, U. Geyer, D. Schelle, E. Kley, A. Tünnermann, U. Lemmer, and M. Gerken, "Optical characterization of photonic crystal slabs using orthogonally oriented polarization filters," Opt. Express **16**, 7153-7160 (2008).
24. G. Alagappan, X. W. Sun, and M. B. Yu, "Out-of-plane diffraction of a two-dimenisonal photonic crystal with finite dielectric modulation," J. Opt. Soc. Am. A **25**, 1098-1103 (2008).
25. B. Cunningham, P. Li, B. Lin, and J. Pepper, "Colorimetric resonant reflection as a direct biochemical assay technique," Sens. Actuators B **81**, 316-328 (2002).
26. B. Cunningham, B. Lin, J. Qiu, P. Li, J. Pepper, and B. Hugh, "A plastic colorimetric resonant optical biosensor for multiparallel detection of label-free biochemical interactions," Sens. Actuators B **85**, 219-226 (2002).
27. I. D. Block, L. L. Chan, and B. T. Cunningham, "Photonic crystal optical biosensor incorporating structured low-index porous dielectric," Sens. Actuators B **120**, 187-193 (2006).
28. N. Ganesh, I. D. Block, and B. T. Cunningham, "Near ultraviolet-wavelength photonic-crystal biosensor with enhanced surface-to-bulk sensitivity ratio," Appl. Phys. Lett. **89**, 023901 (2006).
29. O. Levi, M. M. Lee, J. Zhang, V. Lousse, S. R. J. Brueck, S. Fan, and J. S. Harris. "Sensitivity analysis of a photonic crystal structure for index-of-refraction sensing," Proc. SPIE **6447**, 2-9 (2007).
30. O. Levi, M. M. Lee, J. Zhang, V. Lousse, S. R. J. Brueck, S. Fan, and J. S. Harris, "Optical Characterization and Sensitivity Evaluation of Guided-Resonances in Photonic Crystal Slabs for Biosensing Applications," Proc. of the Conference on Lasers and Electro-Optics (CLEO), May 2007.
31. O. Levi, T. T. Lee, M. M. Lee, S. J. Smith, and J. S. Harris, "Integrated semiconductor optical sensors for cellular and neural imaging," Appl. Opt. **46**, 1881-1889 (2007).
32. S. G. Johnson, "Meep", http://ab-initio.mit.edu/wiki/index.php/Meep

1. Introduction

The ability to detect small changes in the refractive index of a biological analyte is very important for the fundamental studies in biological and chemical sciences, as well as applications such as point-of-care diagnostics and defence. Various label-free biosensor technologies utilizing micro-mechanical systems, surface plasmon resonance excitation,[1–3] as well as guided-mode resonance effects[4–31] have been recently developed with a main goal of reducing measurement complexity, increasing sensitivity and reducing cost. Furthermore, miniaturization of biological analysis systems makes the detection system portable, which is of particular interest for the bio-medical and defence sectors.

In this respect all-dielectric photonic crystal (PhC) bio-sensors operating on the principles of guided-mode resonance[4–31] promise great potential by offering high degree of miniaturization and high sensitivity. In a typical implementation of such a sensor, PhC slab is designed as to exhibit resonant transmission (or reflection) when illuminated perpendicular to the plane of a

#101181 - $15.00 USD Received 5 Sep 2008; revised 17 Oct 2008; accepted 17 Oct 2008; published 21 Oct 2008

slab.[25–31] As was demonstrated in,[6,11,18] when a plane wave with a frequency of a guided-mode resonance is incoming onto a PhC slab, such a wave excites a long living radiative state localized within a PhC. Resonant frequency of such a state is typically highly sensitive to the geometrical and material parameters of a PhC slab, which is a principal reason for utilizing such resonances for sensing. Practically, sensing is performed via detection of the spectral shifts in the peak positions for small changes of a measurand.

In particular, for the PhC sensors featuring a square lattice of holes etched in a thin dielectric slab, theoretical studies of a spectrum of resonances as a function of the lattice constant and the slab thickness were reported in.[13,18] Later, Levi et al.[29–31] have presented optical characterization of a PhC slab sensor using guided-mode resonances, and sensitivities of $\Delta\lambda/\Delta n = 130$ nm/RIU around 816 nm were reported. This particular choice of a sensor geometry was motivated by the capabilities of an e-beam lithography technique that was used to fabricate the sensor prototype.

In this paper, we report several sensor designs based on PhC slabs consisting of either a monolayer of a triangular lattice of silica beads embedded into a dielectric slab placed on top of a substrate (see Fig. 1(a)), or, alternatively, spherical voids embedded into a dielectric suspended on one side in air (see Fig. 1(b)). We then characterize the sensitivity of the guided-mode resonances in such systems to the changes in the refractive index of analyte covering the PhC slab. Our work is motivated by recent progress in the field of PhC fabrication by self assembly of sub-micron spheres followed by backfilling of the inter-sphere voids, and optional subsequent etching of the spheres. To our knowledge, effects of structure parameters on guided-mode resonances in such structures have not yet been reported. Moreover, we find that sensitivities in the spherical voids structures can be several times as high as in the case of classical PhC slabs featuring a square array of cylindrical holes.

The work is organized as follows. In Section 2 we begin with a description of the simulation model and method. Study of the reflection spectra of various PhC slabs is presented in Section 3. Section 4 is devoted to the parameter optimization. The optimal slab thickness and effect of the analyte thickness on sensor sensitivity are discussed.

2. Simulation model and method

In this paper we make simulations for the two types of structures related to the experiments currently in progress in our laboratories. For the fabrication of both structures one starts with a self-assembled hexagonally close packed monolayer of silica beads on silicon substrate. The interstitial region between the beads can then be infiltrated with another material (silicon nitride in our case), which we refer to later in the paper as the slab material. As a last step, the whole structure can finally be terminated with a small cap of the same material as used for infiltration, thus resulting in a structure shown in Fig. 1(a). To create the second structure, one starts with a structure of Fig. 1(a) and then selectively removes the silicon substrate, and after that silica beads, thus resulting in an inverted structure shown in Fig. 1(b).

Our simulations are performed by the Meep implementation of the finite-difference time-domain (FDTD) method.[32] Figure 1 shows the computation domains that were constructed to calculate the normal incidence reflection spectra. The cyan, red, black and blue, respectively, denote the liquid, silica beads, substrate and dielectric slab material. All the feature sizes are defined in terms of a lattice constant a. The bead radius in a hexagonally close packed lattice is $r = 0.5a$. The liquid above beads can be finite or infinite. The refractive index of liquid is taken to be in the vicinity of 1.3. The refractive index of silica used in this article is assumed to be 1.45. For the substrate, a general value of 3.2 is taken (case of semiconductor) and the absorption is neglected for simplicity. Unless stated otherwise, the cap above the monolayer of beads has a size $t = 0.4a$, and is of the same material as the one used for filling the inter-bead

#101181 - $15.00 USD Received 5 Sep 2008; revised 17 Oct 2008; accepted 17 Oct 2008; published 21 Oct 2008

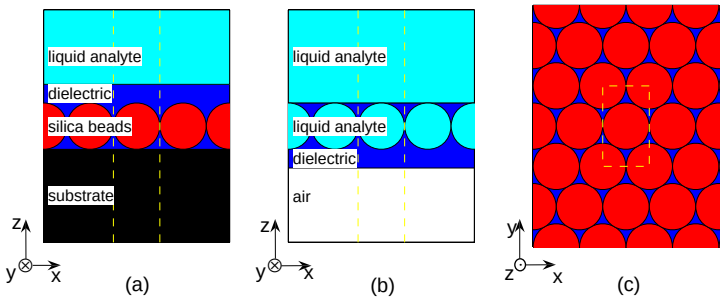

Fig. 1. Schematics of photonic crystal slab sensors based on guided-mode resonances. The area surrounded by yellow dash line denotes a single crystal unit cell. (a) Monolayer silica beads (red) inside a dielectric slab (blue) on substrate (black). The cyan denotes liquid analyte. (b) Monolayer analyte-filled spherical voids (cyan) inside a dielectric slab (blue). (c) Cross section of structures in (a) and (b) in the *xy* plane.

spacing.

The computation domain includes a single crystal unit cell as shown in Fig. 1(c). On the surfaces which are perpendicular to the z direction, we impose the Perfectly Matched Layer (PML) absorbing boundary conditions. For the remaining four surfaces, we impose a Bloch periodic boundary condition. The incident source is a Gaussian pulse source placed at a plane perpendicular to the z direction and the light propagates along the z direction. The electric field of the source is polarized along the y direction, although similar results (not reported) are obtained for the other polarization. In simulation we use the normalized frequency which is always specified in units of $2\pi c/a$, that is, a/λ. c is the light velocity in the free space and λ is the wavelength. In order to get normal-incidence reflection coefficient (the reflected flux divided by the incident flux), we perform two simulations, one with and another without the PhC slab (for the details of the method see the Meep manual [32]).

3. Simulation and analysis

3.1. PhC slabs containing silica beads

First we consider reflection spectra of PhCs featuring silica beads (Fig. 1(a)) embedded into a dielectric slab. In our simulations we vary the refractive index of a slab material from 1.1 to 3.3 (blue area in Fig. 1). Using the computational setup as described above, we calculate the reflection spectra of the structure displayed in Fig. 1(a). The results are shown in Fig. 2. The solid blue and dashed green curves are, respectively, for the two values 1.30 and 1.33 of the analyte refractive index. Difference between these two curves is an indicator to the sensitivity of the reflection spectra to the changes in the analyte refractive index. Figure 2 shows that there are no guided-mode resonances for PhCs with the slab material of small refractive index (eg: $n = 1.1, 1.3, 1.5$), due to a small refractive index contrast between the beads and the slab. For a strong refractive index contrast, however, the guided-mode resonances start appearing in the reflection spectrum. One also observes a sizable spectral shift of the resonance peaks for the two different values of the analyte refractive index. For example, from Fig. 2 it follows that if the diameter of beads is 500 nm, then for the slab refractive index 2.1 the shift of the first resonance peak is 1.9 nm for the 0.03 RIU change in the analyte refractive index (solid blue and dashed green curves) which yields the sensitivity of $\Delta\lambda/\Delta n = 63$ nm/RIU at the operation wavelength of ~ 820 nm. It is typically a safe assumption that a 0.1 nm change in the position of

#101181 - $15.00 USD Received 5 Sep 2008; revised 17 Oct 2008; accepted 17 Oct 2008; published 21 Oct 2008

a resonance peak can be detected reliably, which leads to a sensor resolution of 1.5×10^{-3} RIU. Such value is, however, quite standard for many medium-resolution refractive index sensors.

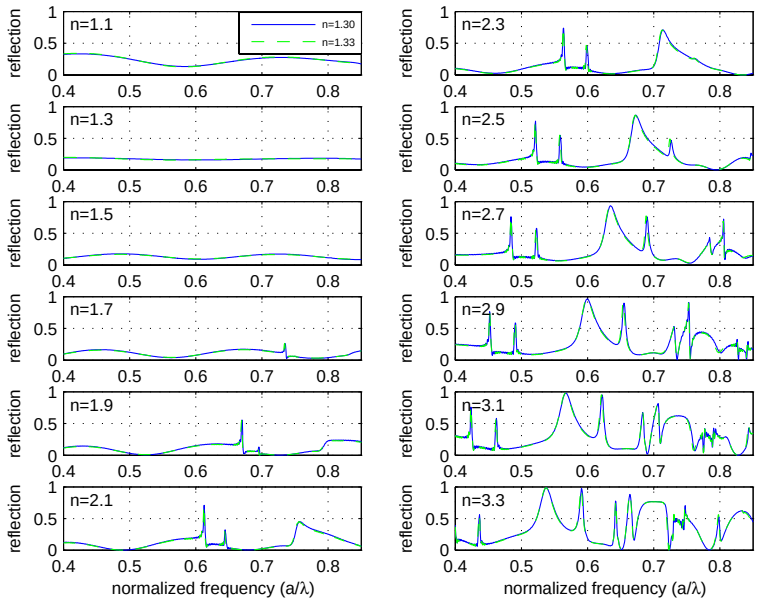

Fig. 2. Reflection spectra from the PhCs featuring silica beads inside a dielectric slab for the various values of slab material refractive index (from 1.1 to 3.3). Solid blue and dashed green curves are respectively for the 1.30 and 1.33 values of the analyte refractive index.

Apparent reason for such a low sensitivity of this PhC slab sensor design is in strong localization of the electromagnetic field of a guided-mode resonance inside a PhC, with only a small overlap with the analyte. Consequently, change in the analyte refractive index would only have a little effect on the electric field of guided-mode resonances and, therefore, would not affect the reflection spectrum. In the next section we find that PhC slabs featuring analyte filled spherical holes show much higher sensitivities due to improved overlap between the guided-mode resonance field and analyte.

3.2. PhC slabs containing spherical voids

The reflection spectra of PhCs featuring analyte-filled spherical voids embedded into a dielectric slab (see Fig. 1(b)) are shown in Fig. 3. The spectra exhibit sharp resonant features when the slab refractive index is higher than 1.6. Moreover, the peak position of guided-mode resonances shifts considerably even for a small change in the analyte refractive index. Particularly, in Fig. 3 solid blue and dashed green curves correspond to the PhC slab reflection spectra for the values 1.30 and 1.33 of the analyte refractive index respectively. As an example, if the bead diameter is 500 nm, for the refractive index 2.0 (a typical value of the refractive index for a silicon nitride material) the difference in the position of the third peak for the solid blue and dashed green curves in Fig. 3 is about 7.4 nm, which defines sensitivity $\Delta\lambda/\Delta n = 246$ nm/RIU at the operation wavelength of ~ 650 nm. This value of sensitivity is twice as large as $\Delta\lambda/\Delta n = 130$ nm/RIU reported in the Ref.[29] With the same assumption that a 0.1 nm change in the position of a resonance peak can be detected reliably, this leads to a

#101181 - $15.00 USD Received 5 Sep 2008; revised 17 Oct 2008; accepted 17 Oct 2008; published 21 Oct 2008

sensor resolution of 4×10^{-4} RIU. Such value is, however, very good for a medium-resolution refractive index sensor. As it will be demonstrated shortly, improvement in the sensor sensitivity is related directly to the improved overlap between the guided-mode resonance field and the analyte.

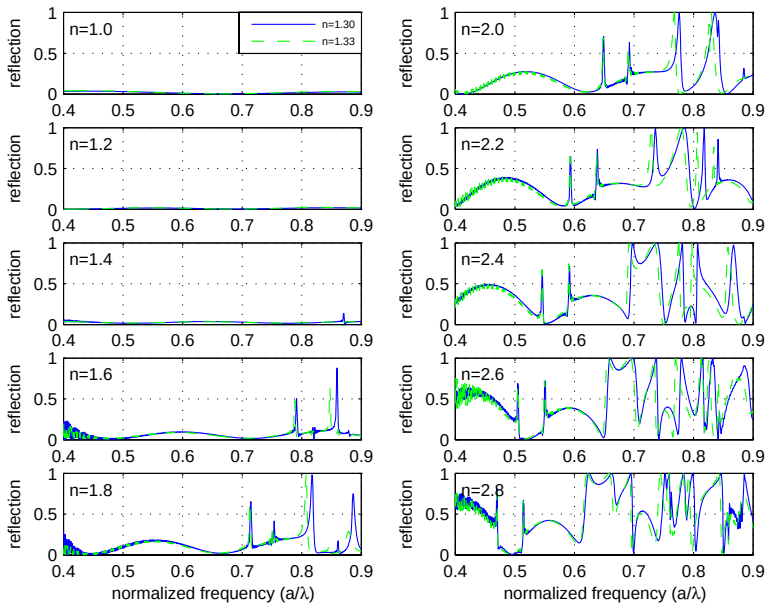

Fig. 3. Reflection spectra from the PhCs featuring analyte-filled spherical voids in a dielectric slab for the various values of the slab material refractive index (from 1.0 to 2.8). Solid blue and dashed green curves are respectively for the 1.30 and 1.33 values of the analyte refractive index.

4. Parameter optimization

In what follows we only consider PhC slabs with embedded triangular lattice of voids. We now study the effects of the slab thickness and analyte thickness on guided-mode resonance properties. Moreover, as one typically finds several guided-mode resonances in the reflection spectra of a PhC slab we investigate why different resonances can have very different sensitivities to the changes in the analyte refractive index. In the following simulations we fix the refractive index of the slab material at 2.05. Experimentally, such refractive index can be realized using silicon nitride deposition process.

4.1. Slab thickness

We start by investigating the effect of a slab thickness on guided-mode resonances. In all our simulations we assume that analyte is infinitely extended on one side of a PhC slab as demonstrated in Fig. 1(b). As before, we perform two simulations for the two values 1.30 and 1.33 of the analyte refractive index. Figure 4 shows the reflection spectra of five PhC slabs, each with a different cap thickness t (see also Fig. 5 for a field distribution at peak 1 and peak 4 resonances). The reflection spectra exhibit a number of important features. Thus, position of all the resonances decrease in normalized frequency as the analyte refractive index increases

#101181 - $15.00 USD Received 5 Sep 2008; revised 17 Oct 2008; accepted 17 Oct 2008; published 21 Oct 2008

from 1.30 to 1.33. There is one resonance, labelled as peak 4, with normalized frequency close to 0.84 (see solid blue curve in Figs. 4(c,d,e)) that displays little variation in width and spectral position as the cap thickness increases from $0.2a$ to $0.4a$, thus been resistant to fabrication imperfections. This resonance is also narrower than others and for $t = 0.2a$ it is far separated from the other closest peak. Finally, this resonance shifts more than others as the liquid index increases from 1.30 to 1.33, thus being the most sensitive to the changes in the analyte refractive index. All these properties make operation in the vicinity of such a peak very suitable for sensing applications.

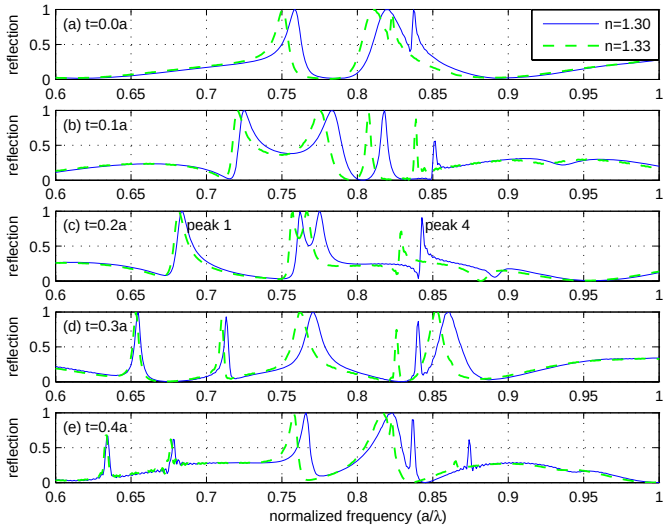

Fig. 4. Reflection spectra of five photonic crystal slabs with various cap thicknesses t. Solid blue and dashed green curves are respectively for the 1.30 and 1.33 values of the analyte refractive index.

For the $t = 0.2a$ design, normalized frequencies a/λ of standing resonances for such a peak are 0.8428 and 0.8292 for the 1.30 and 1.33 values of the analyte refractive index (solid blue and dashed green curves). If the lattice constant a is 500 nm, sensitivity associated with this peak is $\Delta\lambda/\Delta n = 327$ nm/RIU which is even better than 246 nm/RIU demonstrated in the last section for the unoptimized structure.

We now compare peak 4 resonance to a more common one, which we denote as peak 1 in Fig. 4 (for $t = 0.2a$ peak 1 normalized frequency is 0.68). Peak 1 is highly sensitive to the slab thickness, and is only moderately sensitive to the changes in the analyte refractive index. The different sensitivity of these two resonances can be understood by considering their correspondent electric field distributions. Thus, in Fig. 5, we plot the instantaneous values of the y components of the electric fields at peak 1 and peak 4 resonances (cap thickness $t = 0.2a$, analyte refractive index 1.30). Normalized frequencies of CW sources used to generate these pictures are respectively 0.6835 and 0.8428. Figure 5(a) shows that the electric field of the mode at peak 1 concentrates most of its electric field in the slab material, while a large part of the electric field (Fig. 5(b)) of the mode at peak 4 is concentrated in the analyte filled void and slab/analyte interface. Therefore, the change of the analyte refractive index affects peak 4 much more strongly than peak 1. We have furthermore simulated distributions of the electric field at resonances in systems with different cap thicknesses, and confirmed that peak 4 insensitivity to

#101181 - $15.00 USD Received 5 Sep 2008; revised 17 Oct 2008; accepted 17 Oct 2008; published 21 Oct 2008

the cap size and high sensitivity to the analyte is related to the very high content of the peak electric field in the analyte.

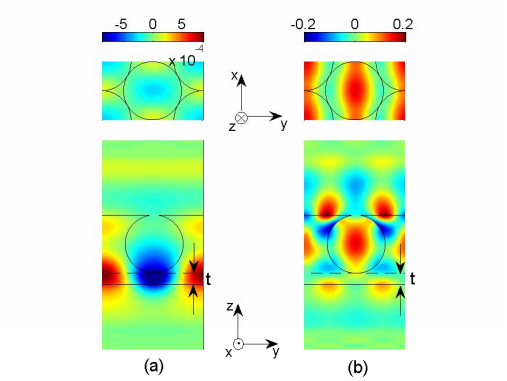

Fig. 5. Distribution of the y component of the electric field for peak 1 and peak 4 across PhC crossection with $t = 0.2a$. The black line denotes the contours of the solid material. In both cases analyte fills the spherical void, as well as the region above it.

4.2. Effect of the finite analyte thickness

So far, we have studied sensing assuming infinitely thick analyte covering a PhC. In this last subsection we investigate the case of an analyte of finite thickness. This scenario is of interest, for example, when trying to minimize the volume of the analyte used, thus operating with thin analyte films. Another interesting question is how thick should the analyte film be to result in effectively a bulk-like response of sensor.

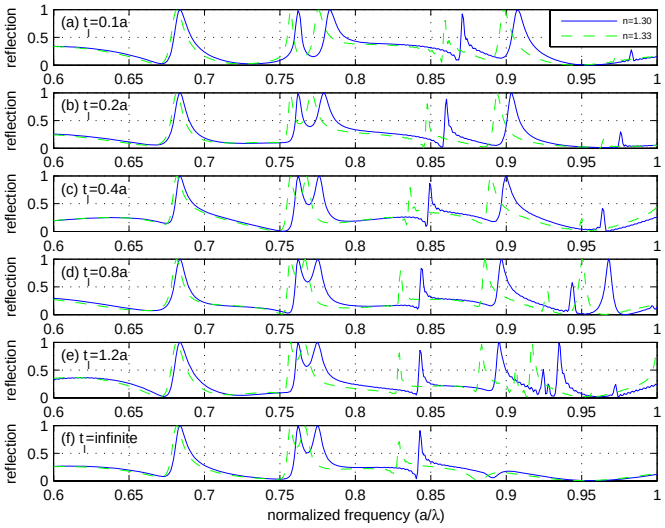

Fig. 6. Reflection spectra of six PhC slabs with different analyte thicknesses t_l : $0.1a$, $0.2a$, $0.4a$, $0.8a$, $1.2a$, ∞.

#101181 - $15.00 USD Received 5 Sep 2008; revised 17 Oct 2008; accepted 17 Oct 2008; published 21 Oct 2008

In order to better understand the effect of analyte thickness, in Fig. 6 we plot the reflection spectra of a PhC slab covered with analyte of different thicknesses t_l (cap thickness is constant and assumed to be $t = 0.2a$). From this figure we observe that resonances with fields strongly confined inside a PhC slab (for example, peak 1 in Fig. 6) do not change strongly their position when analyte thickness is varied. On the other hand, resonances with fields having large fraction in the analyte (for example, peak 4 in Fig. 6 with normalized frequency around 0.85 for $t_l = 0.2a$) do change their position when analyte thickness is varied. We further plot the peak 4 position versus the analyte thickness t_l in Fig. 7, where the dashed line (normalized frequency 0.8428) denotes the peak position in an infinite analyte. From Fig. 7 we conclude that spectral position of such a peak becomes close to its bulk position for the analyte thickness larger than $0.6a$, at which peak position deviation from the bulk becomes less than 1%. The reason for such a behavior it simple to rationalize. Guided-mode resonances are modes with electromagnetic energy, generally, localized in the near vicinity of a PhC slab. If t_p is a characteristic penetration depth of a resonance field into a bulk analyte, then as long as the analyte thickness is larger than t_p, modal properties of a guided-mode resonance will stay unchanged and bulk-like.

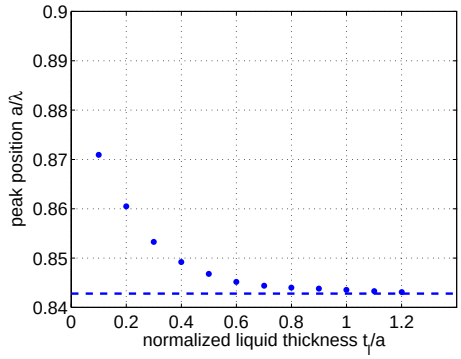

Fig. 7. Peak position versus normalized thickness t_l/a of an analyte. The dashed line denotes the peak position for an infinite analyte.

To support this argument, in Fig. 8 we present distributions of the y component of an electric field for the peak 4 resonance for the different analyte thicknesses t_l: $0.1a$, $0.4a$, $1.2a$ and infinite thickness. First, we confirm that for any analyte thickness a significant part of the modal energy is in the analyte. We also confirm that electric fields of guided-mode resonances decay fast with the distance from the PhC slab. Therefore, when the analyte thickness, for example, exceeds $1.2a$ (plot (c) in Fig. 8), the outer analyte boundary does not affect field distribution in the resonance mode. This signifies that guided-mode resonances in a system with analyte of thicknesses larger than $\sim a$ are similar to the guided-mode resonances in a system with infinite analyte.

5. Conclusion

Using the finite-difference time-domain method, we investigated two resonant PhC slab sensor designs for sensing changes in the analyte refractive index. Suggested guided-mode resonance sensors comprise a monolayer of hexagonally closed-packed silica beads or spherical voids placed inside of a dielectric slab. We show that the most sensitive design is based on voids filled with analyte. In such sensors some guided-mode resonances have a substantial fraction of their electro-magnetic energy localized in the analyte, thus enabling designs with spectral sensitivity as high as 327 nm/RIU at 600 nm operation wavelength.

#101181 - $15.00 USD Received 5 Sep 2008; revised 17 Oct 2008; accepted 17 Oct 2008; published 21 Oct 2008

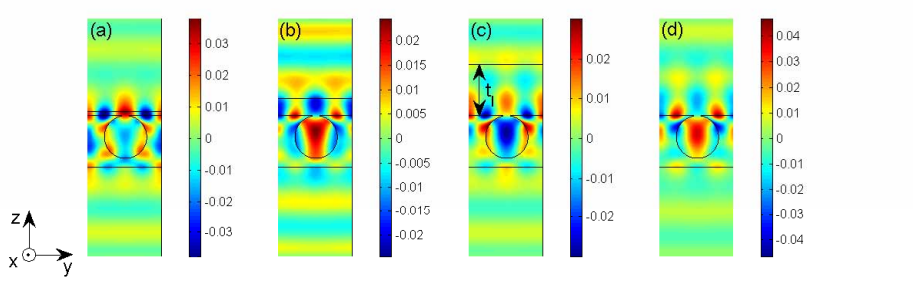

Fig. 8. Distribution of the y component of the electric field for peak 4 across PhC crossection with $t = 0.2a$ and various thicknesses of the analyte layer t_l: (a) $0.1a$, (b) $0.4a$, (c) $1.2a$, (d) ∞. The black lines denote the contours of the solid material and analyte. In both cases analyte fills the spherical void.

Acknowledgment

This work was supported by the Natural Sciences and Engineering Research Council of Canada, Strategic Grant 336830 2006.

#101181 - $15.00 USD Received 5 Sep 2008; revised 17 Oct 2008; accepted 17 Oct 2008; published 21 Oct 2008